CONF-850533--2

**LA-UR** -85-1477

Los Alamos National Laboratory is operated by the University of California for the United States Department of Energy under contract W-7405-ENG-36

TITLE BISMUTH GERMANATE SCINTILLATORS: APPLICATIONS IN NUCLEAR SAFEGUARDS AND HEALTH PHYSICS

AUTHOR(S) C. E. Moss
E. J. Dowdy
M. C. Lucas

LA-UR--85-1477

DE85 010730

SUBMITTED TO Sixth Symposium on X- and Gamma-Ray Sources and Applications
Ann Arbor, Michigan
May 21-23, 1985

## DISCLAIMER



Los Alamos National Laboratory
Los Alamos, New Mexico 87545

# BISMUTH GERMANATE SCINTILLATORS: APPLICATIONS IN NUCLEAR SAFEGUARDS AND HEALTH PHYSICS

C. E. Moss, E. J. Dowdy, and M. C. Lucas

Los Alamos National Laboratory
P.O. Box 1663, MS J562
Los Alamos, NM 87545

## ABSTRACT

Bismuth germanate (BGO) scintillators are preferable to NaI(Tl) scintillators or germanium detectors for some applications. We describe two systems based on BGO scintillators for applications in nuclear safeguards and health physics. The first system, which consists of eight scintillators and a computer-based data acquisition system, is very efficient. The second, which consists of one scintillator and a small analyzer, is less efficient but portable. A computer code that uses measured response functions and photopeak efficiencies, unfolds the BGO distributions measured with these systems to determine gamma-ray flux spectra and dose rates. One application of these systems is the accurate determination of flux spectra and dose rates from containers of uranium or plutonium. A second application determined these quantities from a replica of Little Boy, the device exploded over Hiroshima.

## 1. INTRODUCTION

Although a high-resolution germanium detector is preferable for most gamma-ray measurements, a scintillation detector is more suitable for some

applications. If a spectrum contains high-energy gamma rays or a continuum that must be unfolded, then a scintillator is often the better choice. Until recently, NaI(Tl) scintillators were preferred.

Now bismuth germanate (BGO) scintillators are replacing NaI(Tl) scintillators in many applications, for several reasons. The photopeak efficiency of BGO scintillators is larger than that of NaI(Tl), especially at high energies (Fig. 1); thus measurements can be performed faster with a BGO scintillator than with a NaI(Tl) scintillator of similar size. Because the BGO photofraction is larger, the gamma-ray pulse-height distributions resulting from BGO scintillators are easier to analyze than distributions from NaI(Tl) scintillators. Moreover, BGO is mechanically and chemically more stable than NaI(Tl) and is highly insensitive to low-energy neutrons.[1]

BGO scintillators are not suitable for some applications. Because the light output from BGO is only about 8% of that from NaI(Tl),[2] the resolution is worse, especially at low energy. The higher efficiency of BGO causes sum peaks to be larger than those from NaI(Tl). The larger temperature coefficient of BGO[3] necessitates better temperature control or gain stabilization. A BGO detector costs more than twice as much as the same size NaI(Tl) detector. The largest BGO detector readily available commercially is 10.16 cm in diameter and 7.62 cm in length.

The Advanced Nuclear Technology Group of the Los Alamos National Laboratory chose BGO scintillators for two systems used in nuclear safeguards and health physics. This paper describes these systems and some applications.

## 2. EQUIPMENT

The first system, which is very efficient, consists of eight BGO scintillators and a dedicated minicomputer. Each BGO scintillator is 7.62 cm in diameter and 7.62 cm in length. Such large crystals were chosen to maximize the photofraction. The detector resolutions at 662 keV range from 13.2 to 19.1% in full width at half maximum. The unshielded scintillators are supported on low mass tripods around a radioactive source so as to minimize scattering. A LeCroy 3500 data acquisition system equipped with a CAMAC crate acquires gamma-ray pulse-height distributions from the eight detectors. Gain stabilizers may be set on gamma-ray peaks in the pulse-height distributions for long measurements. In addition to the eight scintillators, one special scintillator equipped with an $^{241}$Am pulser is available for measurements of distributions that do not have suitable peaks for stabilizing. Figure 2 shows our eight-scintillator system set up around a transuranic waste assay system that uses a deuterium-tritium generator for active interrogation of the waste.[4]

The second system, which is portable, consists of a single scintillator and a small multichannel analyzer (Fig. 3). The Canberra 10 analyzer has 4096

channels and a built-in amplifier, high-voltage supply, and stabilizer. A small cassette recorder stores the data.

## 3. CALIBRATION AND ANALYSIS

We calibrated the system from 0.12 to 8.29 MeV using radioactive sources and reactions. The gamma-ray "point" sources used were $^{57}Co$, $^{139}Ce$, $^{203}Hg$, $^{51}Cr$, $^{113}Sn$, $^{7}Be$, $^{85}Sr$, $^{137}Cs$, $^{54}Mn$, $^{88}Y$, $^{65}Zn$, $^{22}Na$, $^{60}Co$, $^{208}Tl$, and $^{16}N$. The reactions used were the $^{9}Be(\alpha,n)^{12}C$ reaction in a plutonium-beryllium source that yields a 4.439-MeV gamma ray and the $^{14}N(p,\gamma)^{15}O$ reaction produced in a Van de Graaff target. The calibration extends above the energies available from long-lived isotopic sources because some materials of interest emit 4.439-MeV gamma rays from the reaction $^{9}Be(\alpha,n)^{12}C$. High-energy neutron capture gamma rays such as the 7.631-7.645-MeV doublet from iron are also present. Details about the determination of the photopeak efficiency curves and the response functions are given in Refs. 5 and 6, respectively.

Our analysis determines the flux distribution dose rate and integral dose rate. A code called GPEEL, which runs on a CDC 7600 computer or a Cray computer, uses the measured detector efficiency and response function in a stripping procedure to calculate the gamma-ray flux in photons/cm$^2$/s as a function of energy from the raw BGO pulse-height distributions. The code then converts the resulting flux distribution to a dose-rate distribution using a

flux-to-dose-rate curve, based on the work of Dimbylow and Francis.[7] The integral over this dose-rate distribution is the total gamma-ray dose rate.

## 4. APPLICATIONS

One application of our system is the determination of flux distributions and dose rates from containers of uranium or plutonium. Figure 4 shows results from a 550-g shell of depleted uranium containing 0.2% $^{235}U$. Prominent peaks from the $^{234m}Pa$ daughter occur at 767, 1001, and 1800 keV. Much of the gamma-ray output from uranium is bremsstrahlung, which is responsible for the continuum out to the 2.3-MeV end point. Figure 5 shows results from a 455-g shell of plutonium containing 2.65% $^{240}Pu$. Complexes of gamma-ray lines produce peaks at 414, 640, and 760 keV. The flux spectra provide experimental checks of Monte Carlo calculations for the gamma-ray emissions. The presence of contaminants, fission products, and room scatter and of uncertainties in the bremsstrahlung theory makes experimental checks important. The dose rates, which are more accurate than those obtained with simple energy-dependent dosimeters, are useful when dose rates must be known accurately because of safety or legal considerations.

A second application is the determination of the flux distribution and dose rate from a replica of Little Boy, the device exploded over Hiroshima, operating as a reactor at low power. To minimize scatter the device was supported outside on a stand so that the core was 4.0 m from the ground when

operating. Figure 6 shows some results at 0.75 m from the center and 90° from the vertical cylindrical axis. The distributions are dominated by the 7.631-7.645-MeV doublet from neutron capture in the massive steel case. Because data concerning the Hiroshima and Nagasaki survivors provide the basis for many of our radiation safety guidelines, it is important to establish the radiation of the Hiroshima explosion. Experimentally determined flux and dose rate, such as these, provide checks of the calculations at low power and increase the confidence in the calculations for the explosion.

REFERENCES

1. O. Häusser, M. A. Lone, T. K. Alexander, S. A. Kushneriuk, and J. Gascon, Nucl. Instr. and Meth. 213 (1983) 301.

2. O. H. Nestor and C. Y. Huang, IEEE Trans. Nucl. Sci. NS-22 (1975) 68.

3. C. L. Melcher, J. S. Schweitzer, A. Liberman, and J. Simonetti, IEEE Trans. Nucl. Sci. NS-32 (1) (1985) 529.

4. J. T. Caldwell, D. A. Close, T. H. Kuckertz, W. E. Kunz, J. C. Pratt, K. W. Haff, and F. J. Schultz, Nuclear Materials Management XII (proceedings issue) (1983) 75.

5. C. E. Moss, E. W. Tisinger, and M. E. Hamm, Nucl. Instr. and Meth. 221 (1984) 378.

6. C. E. Moss, E. J. Dowdy, A. E. Evans, M. E. Hamm, M. C. Lucas, and E. R. Shunk, Nucl. Instr. and Meth. 219 (1984) 558.

7. P. J. Dimbylow and T. M. Francis, "A Calculation of the Photon Depth-Dose Distributions in the ICRU Sphere for a Broad Parallel Beam, A Point Source, and an Isotropic Field," National Radiological Protection Board report R92, Harwell, England (1979).

## FIGURE CAPTIONS

Figure 1. Comparison of the absolute photopeak efficiency at 30 cm of a BGO and a NaI(Tl) scintillator, each 7.62 cm in diameter and 7.62 cm long.

Figure 2. Array of eight BGO scintillators supported on tripods around a transuranic assay system. The LeCroy 3500 data acquisition system and the NIM bin electronics are on the right.

Figure 3. Portable system consisting of a single BGO scintillator on a tripod and a Canberra 10 multichannel analyzer. The cassette recorder is the small unit in front of the analyzer.

Figure 4. Binned pulse-height distribution (top), flux distribution (middle), and dose-rate distribution (bottom) from a 550-g shell of depleted uranium. Each major peak is labeled with the energy in keV and the radioactive nuclide.

Figure 5. Binned pulse-height distribution (top), flux distribution (middle), and dose-rate distribution (bottom) from a 455-g shell of plutonium.

Figure 6. Binned pulse-height distribution (top), flux spectrum (middle), and dose-rate spectrum (bottom) at (90°, 0.75 m) from the Little Boy replica. The 7.6-MeV peak from Fe(n,$\gamma$) is the most prominent feature of the distribution.

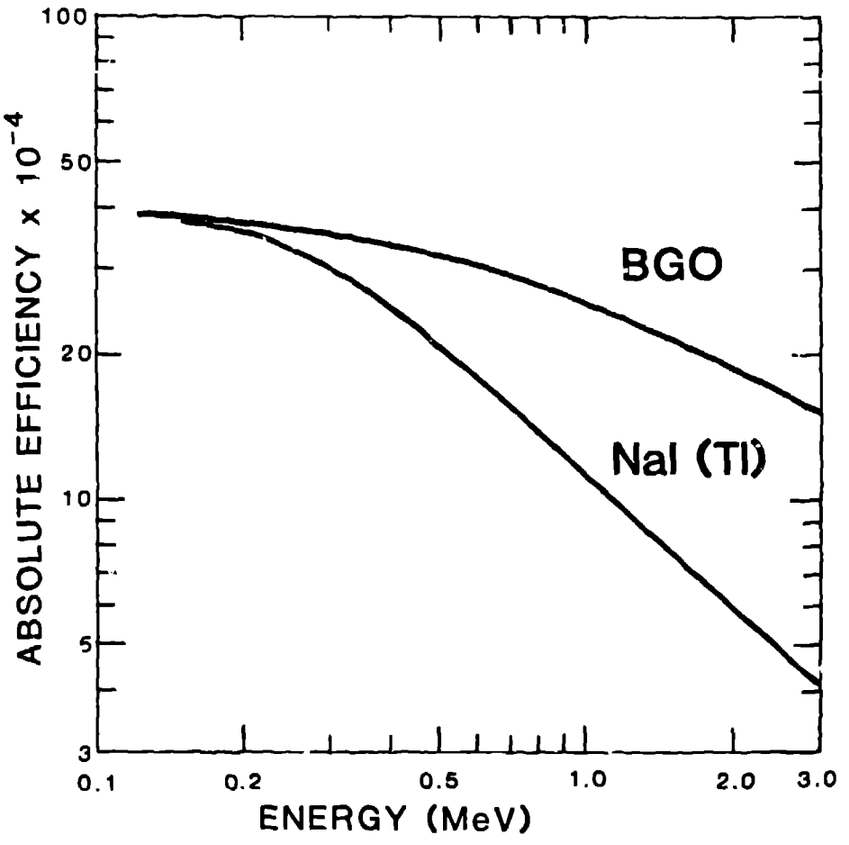
100
50
20
10
5
3
ABSOLUTE EFFICIENCY x $10^{-4}$
BGO
NaI (Tl)
0.1
0.2
0.5
1.0
2.0
3.0
ENERGY (MeV)

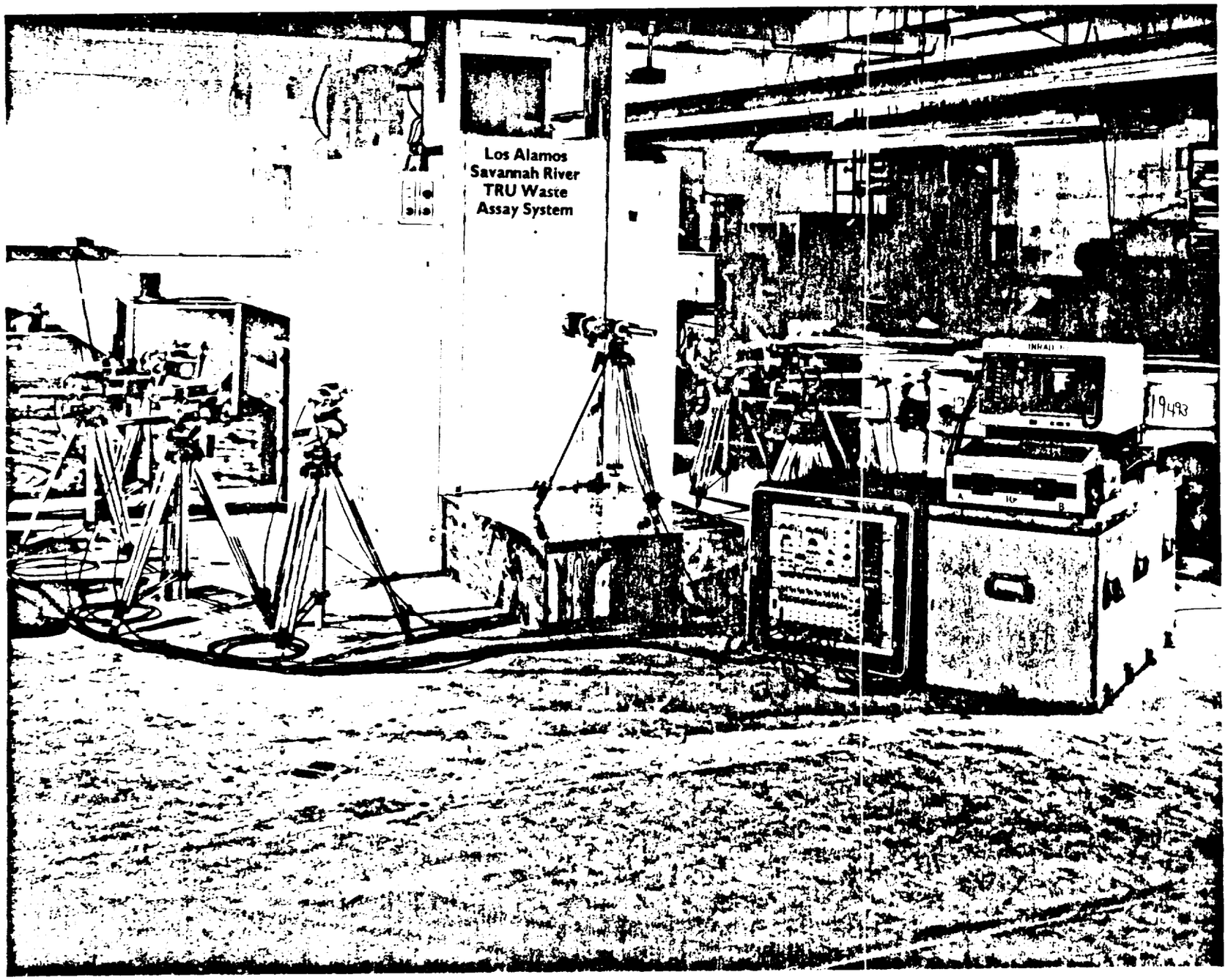
Los Alamos
Savannah River
TRU Waste
Assay System

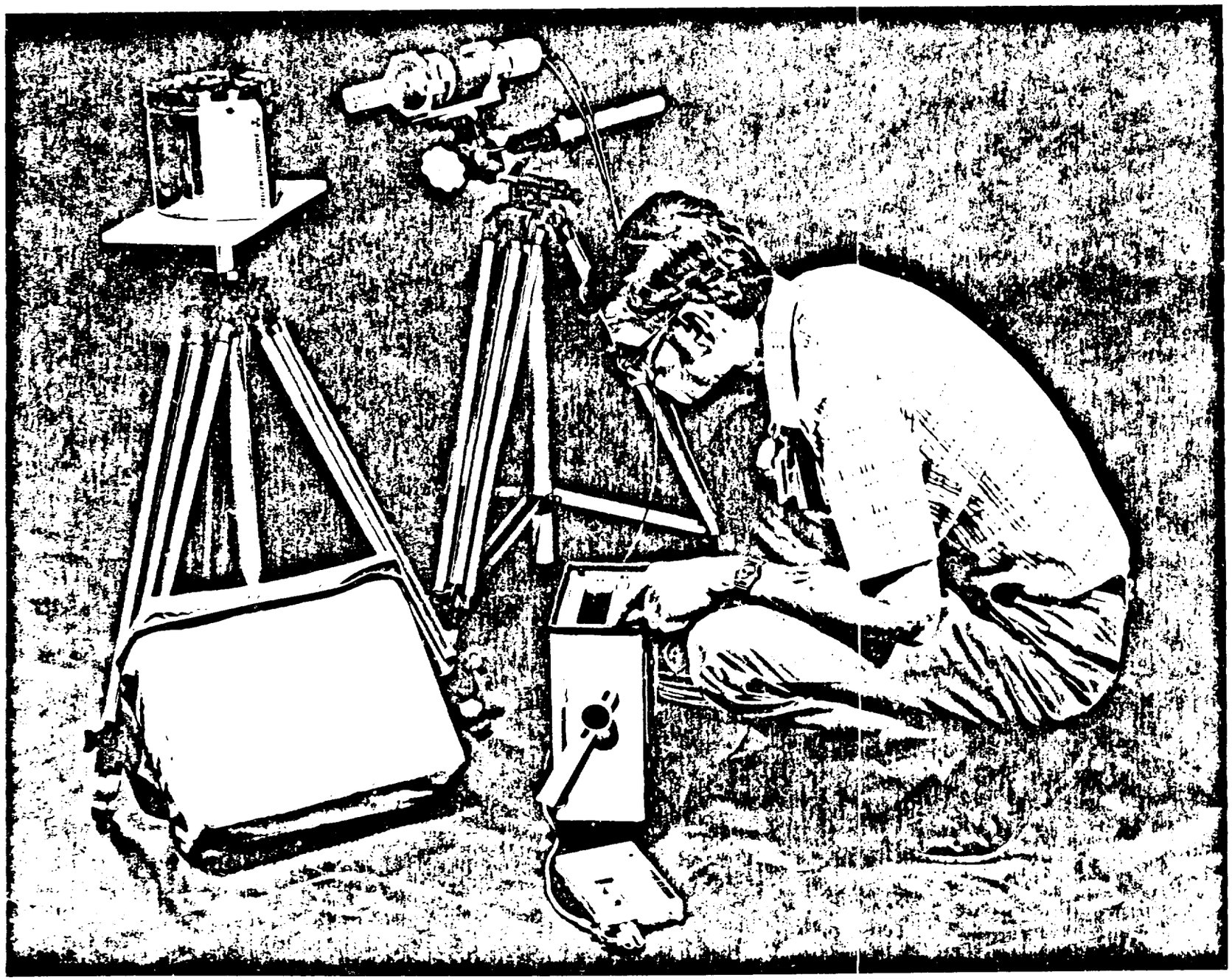
RADIOACTIVE MATERIAL

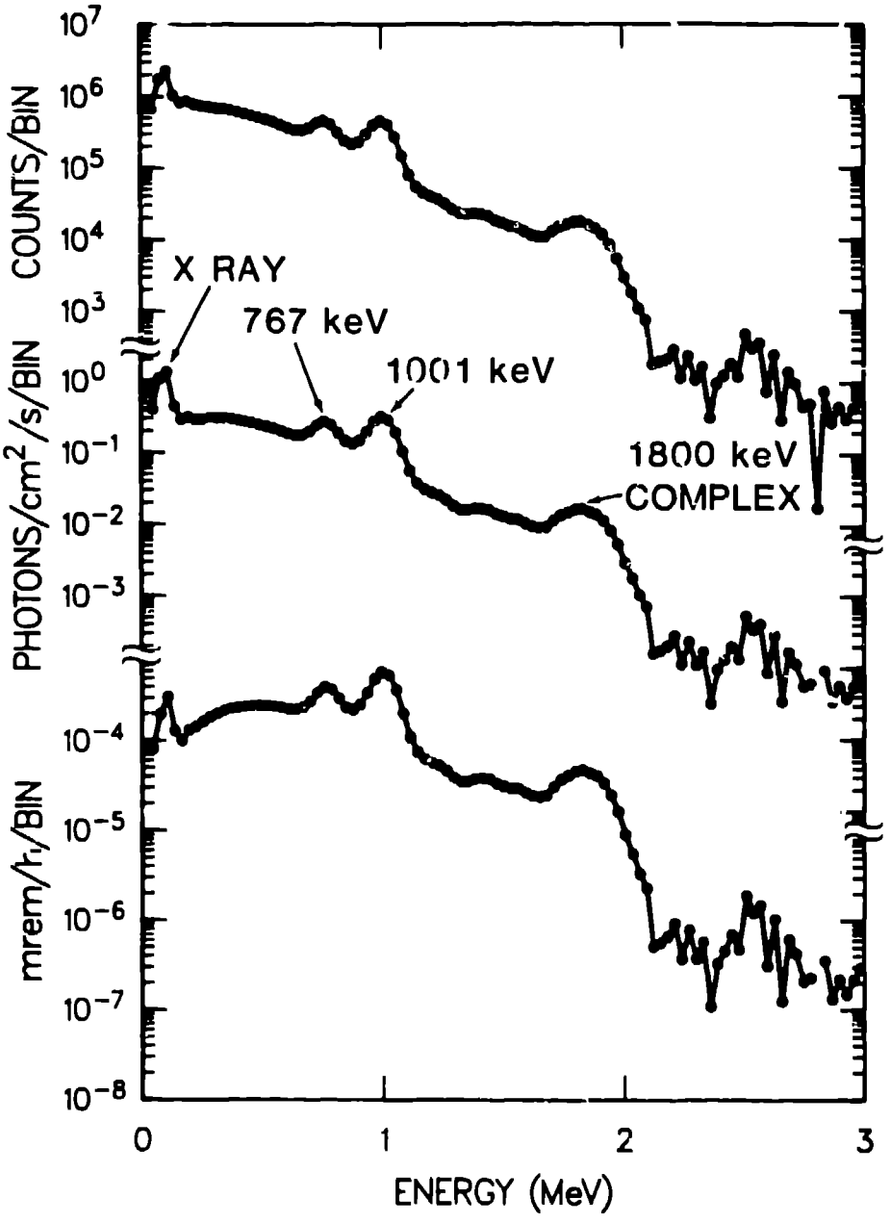
$10^7$
$10^6$
$10^5$
$10^4$
$10^3$
$10^0$
$10^{-1}$
$10^{-2}$
$10^{-3}$
$10^{-4}$
$10^{-5}$
$10^{-6}$
$10^{-7}$
$10^{-8}$
COUNTS/BIN
PHOTONS/cm$^2$/s/BIN
mrem/hr/BIN
X RAY
767 keV
1001 keV
1800 keV
COMPLEX
0
1
2
3
ENERGY (MeV)

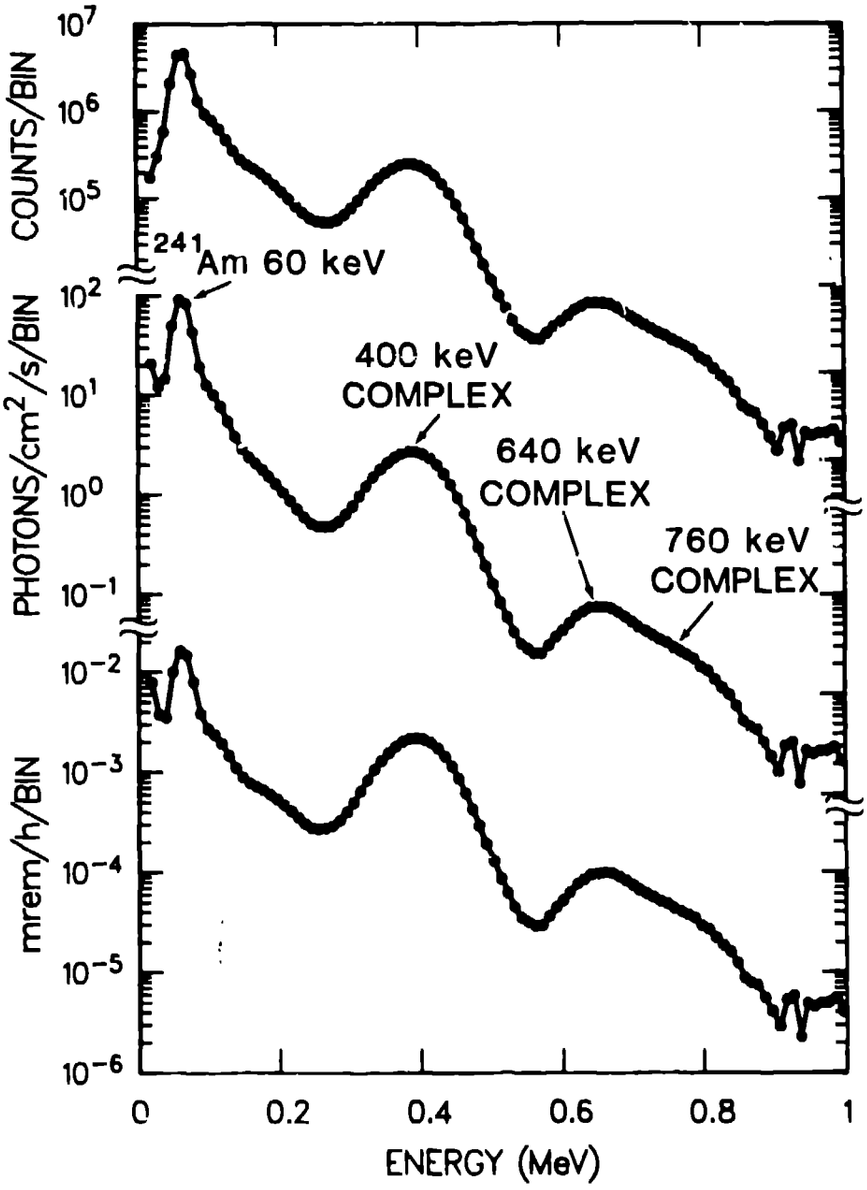
COUNTS/BIN
PHOTONS/cm²/s/BIN
mrem/h/BIN
10⁷
10⁶
10⁵
10²
10¹
10⁰
10⁻¹
10⁻²
10⁻³
10⁻⁴
10⁻⁵
10⁻⁶
241Am 60 keV
400 keV COMPLEX
640 keV COMPLEX
760 keV COMPLEX
0
0.2
0.4
0.6
0.8
1
ENERGY (MeV)

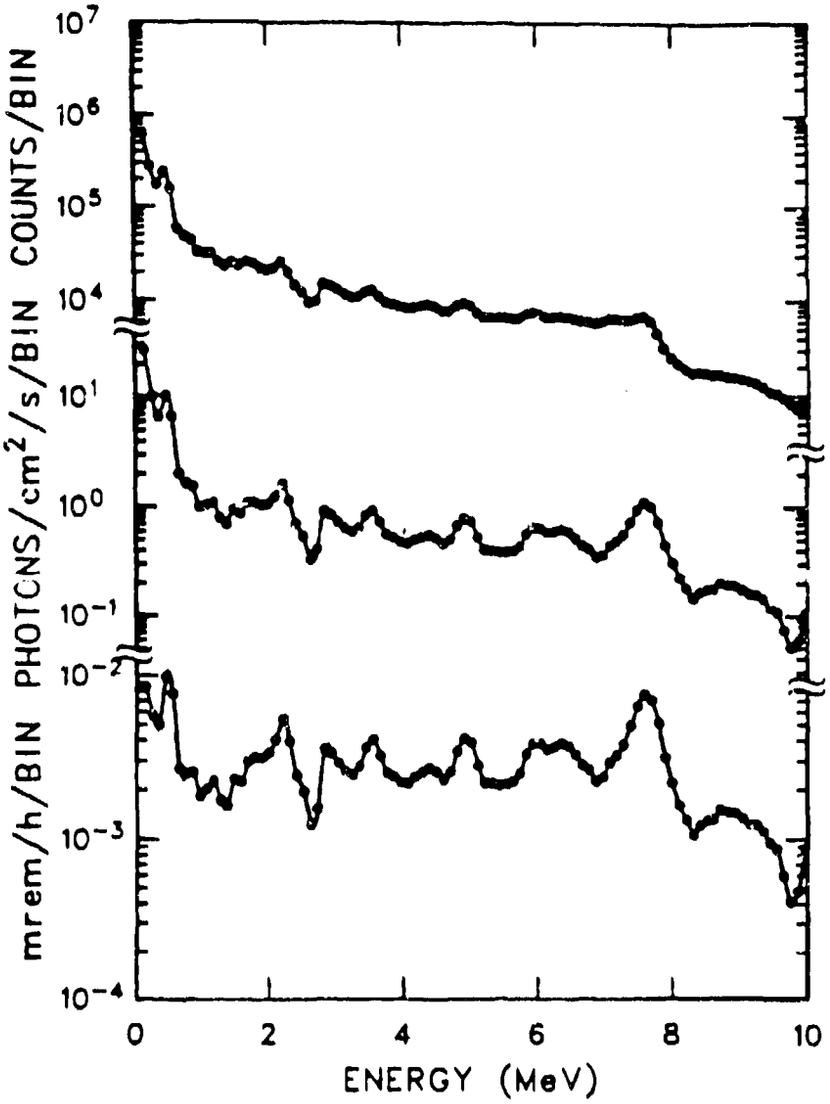
mrem/h/BIN PHOTONS/cm²/s/BIN COUNTS/BIN
10⁷
10⁶
10⁵
10⁴
10¹
10⁰
10⁻¹
10⁻²
10⁻³
10⁻⁴
0
2
4
6
8
10
ENERGY (MeV)